Luminescent Organic Semiconducting Langmuir Monolayers

Agina, Elena V.; Mannanov, Artur A.; Sizov, Alexey S.; Vechter, Olga; Borshchev, Oleg V.; Bakirov, Artem V.; Shcherbina, Maxim A.; Chvalun, Sergei N.; Konstantinov, Vladislav G.; Bruevich, Vladimir V.

Published in:
ACS Applied Materials & Interfaces

DOI:
10.1021/acsami.7b01919

Publication date:
2017

ACS APPLIED MATERIALS & INTERFACES

Research Article

www.acsami.org

Luminescent Organic Semiconducting Langmuir Monolayers

Elena V. Agina,[†,‡] Artur A. Mannanov,[‡,§] Alexey S. Sizov,[†,‡] Olga Vechter,[∥] Oleg V. Borshchev,[†,‡] Artem V. Bakirov,[†,⊥] Maxim A. Shcherbina,[⊥,#] Sergei N. Chvalun,[†,⊥] Vladislav G. Konstantinov,[‡] Vladimir V. Bruevich,[‡] Oleg V. Kozlov,[‡,§] Maxim S. Pshenichnikov,[§] Dmitry Yu. Paraschuk,*[,‡] and Sergei A. Ponomarenko*[,†,‡]

[†]Institute of Synthetic Polymeric Materials of the Russian Academy of Sciences, Profsoyuznaya street 70, 117393 Moscow, Russia

[‡]Faculty of Physics & International Laser Center, Lomonosov Moscow State University, 119991 Moscow, Russia

[§]Zernike Institute for Advanced Materials, University of Groningen, Nijenborgh, Groningen 4 9747 AG, The Netherlands

[∥]Department of Organic Chemistry III/Macromolecular Chemistry, Ulm University, Albert-Einstein-Allee 11, 89081 Ulm, Germany

[⊥]National Research Centre "Kurchatov Institute", Akademika Kurchatova pl. 1, Moscow 123182, Russia

[#]Moscow Institute of Physics and Technology, 4 Institutsky line, 141700 Dolgoprudny, Moscow Region, Russian Federation

Supporting Information

ABSTRACT: In recent years, monolayer organic field-effect devices such as transistors and sensors have demonstrated their high potential. In contrast, monolayer electroluminescent organic field-effect devices are still in their infancy. One of the key challenges here is to create an organic material that self-organizes in a monolayer and combines efficient charge transport with luminescence. Herein, we report a novel organosilicon derivative of oligothiophene−phenylene dimer **D2-Und-PTTP-TMS** (D2, tetramethyldisiloxane; Und, undecylenic spacer; P, 1,4-phenylene; T, 2,5-thiophene; TMS, trimethylsilyl) that meets these requirements. The self-assembled Langmuir monolayers of the dimer were investigated by steady-state and time-resolved photoluminescence spectroscopy, atomic force microscopy, X-ray reflectometry, and grazing-incidence X-ray diffraction, and their semiconducting properties were evaluated in organic field-effect transistors. We found that the best uniform, fully covered, highly ordered monolayers were semiconducting. Thus, the ordered two-dimensional (2D) packing of conjugated organic molecules in the semiconducting Langmuir monolayer is compatible with its high-yield luminescence, so that 2D molecular aggregation per se does not preclude highly luminescent properties. Our findings pave the way to the rational design of functional materials for monolayer organic light-emitting transistors and other optoelectronic devices.

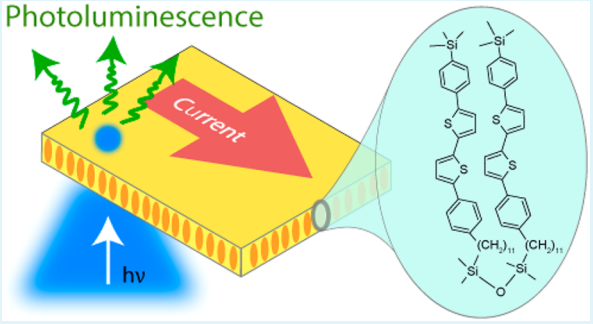

KEYWORDS: *thiophene−phenylene co-oligomers, photoluminescence, Langmuir−Blodgett and Langmuir−Schaefer monolayers, OFETs, organic electronics*

INTRODUCTION

Organic field-effect transistors (OFETs) form a general platform for the new generation of lightweight, flexible, and cheap electronics such as various sensors,[1−5] logic circuits,[6−8] photodetectors,[9−11] and so on. For light-emitting organic electronic devices, the planar OFET architecture is the most promising because it enables higher electroluminescent quantum efficiency of organic light-emitting transistors (OLETs) as compared to the already commercialized OLEDs.[12−14] This promise is still to be fulfilled, however.

The electrical current in organic field-effect devices, such as OFETs and OLETs, flows within a few-nanometer-thick surface layer of the active material adjacent to the dielectric; this fact drives the progress in monolayer organic electronics.[15−21] Ultrathin films are very beneficial for light-emitting field-effect devices as they are free of waveguiding effects that reduce the light output from thick light-emitting devices (OLEDs and OLETs). However, realization of electroluminescence in a monolayer device presents a formidable challenge.

One of the problems is molecular aggregation, which commonly results in luminescence quenching. Recently, Gholamrezaie et al. showed that photoluminescence (PL) of a self-assembled oligothiophene monolayer decreases dramatically with increasing monolayer coverage (growth time).[22] Therefore, selection of appropriate organic molecules for efficient luminescent semiconducting monolayers is of the utmost importance. From the materials point of view, thiophene−phenylene co-oligomer- (TPCO-) based materials

Received: February 9, 2017
Accepted: May 10, 2017
Published: May 10, 2017

DOI: 10.1021/acsami.7b01919
ACS Appl. Mater. Interfaces 2017, 9, 18078−18086

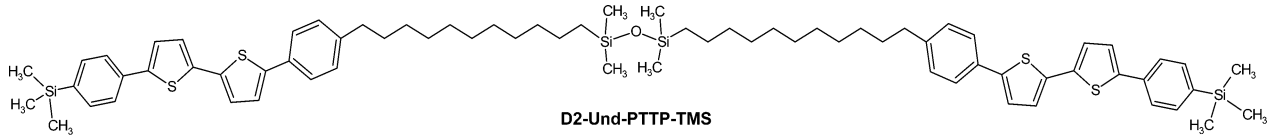

Figure 1. Chemical structure of the oligothiophene−phenylene dimer **D2-Und-PTTP-TMS**.

Scheme 1. Synthesis of D2-Und-PTTP-TMS

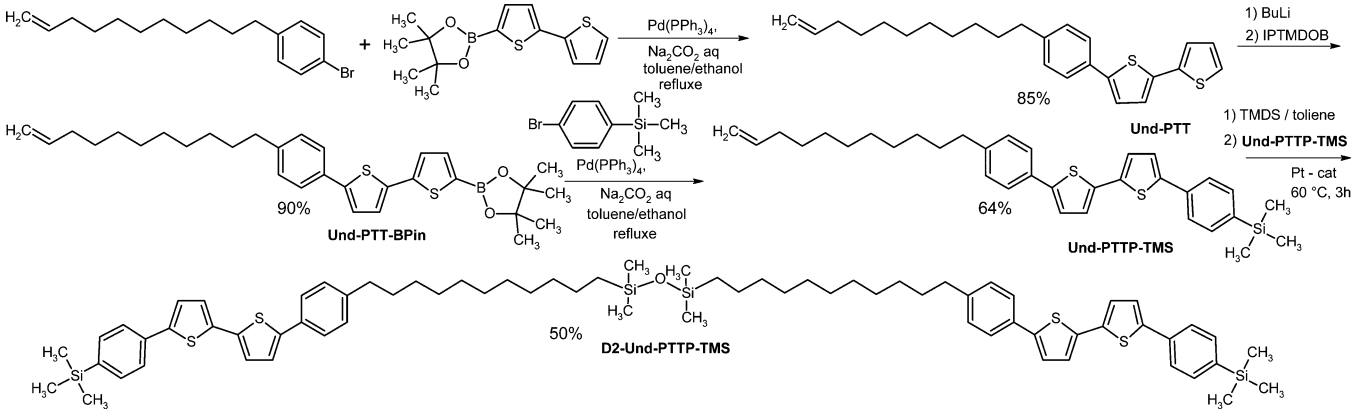

look attractive because of their success in single-crystal OLETs.[23−25]

As for monolayer device fabrication, Langmuir techniques are advantageous because they allow for the fast and robust self-assembly of organic semiconducting monolayers as a technological alternative to many-hours-long self-assembly from solution.[26] Organosilicon derivatives of oligothiophenes or benzothieno[3,2-*b*][1]-benzothiophene (BTBT) have demonstrated the best performance in Langmuir monolayer OFETs.[27−30] However, neither oligothiophenes nor BTBT show significant luminescence in films.

Note that luminescent Langmuir films can be prepared from transition-metal complexes;[31] however, these films do not show any semiconducting properties. Even though the Langmuir technique was used earlier for the preparation of thin films of quinquethiophene or poly(3-hexylthiophene) mixed with arachidic acid in a molar ratio of 60:40 (because, in pure form, these materials do not form any Langmuir films) for organic light-emitting diodes (i.e., for semiconducting and luminescent films), those films were not individual monolayers (they contained from 3 to 45 monolayers) and showed extremely weak (<0.01%) electroluminescence quantum yields.[32−34]

Herein, we demonstrate that ordered two-dimensional (2D) packing of organic conjugated molecules in a semiconducting Langmuir monolayer is compatible with its pronounced luminescence. Using a novel organosilicon derivative of a TPCO, we demonstrate that strong 2D molecular aggregation is not an obstacle for highly luminescent semiconducting monolayers and that the PL quantum yield in the 2D ordered monolayer is considerably higher than that in a polycrystalline three-dimensional (3D) packing of the spin-cast film.

RESULTS AND DISCUSSION

The oligothiophene−phenylene dimer, 1,3-bis[11-(4-{5′-[4-(trimethylsilyl)phenyl]-2,2′-bithien-5-yl}phenyl)undecyl]-1,1,3,3-tetramethyldisiloxane, **D2-Und-PTTP-TMS** (Figure 1), was designed and synthesized as described below. The trimethylsilyl groups [$Si(CH_3)_3-$] provide good solubility of the material in widely used organic solvents and improve its air stability. The tetramethyldisiloxane [$-Si(CH_3)_2-O-Si(CH_3)_2-$] group enables self-assembling monolayer film formation by Langmuir techniques.[27,29] The conjugated oligothiophene−phenylene fragment (PTTP) is responsible for luminescent and semiconducting properties.

The synthesis of compound **D2-Und-PTTP-TMS** is shown in Scheme 1. The first step was the preparation of 5-(4-undec-10-en-1-yl-phenyl)-2,2′-bithiophene (**Und-PTT**) by Suzuki cross-coupling between 1-bromo-4-undec-10-enyl-benzene[35] and 2-(2,2′-bithien-5-yl)-4,4,5,5-tetramethyl-1,3,2-dioxaborolane.[36] After purification by column chromatography on silica gel, **Und-PTT** was obtained as a colorless solid in 85% isolated yield. Subsequent lithiation of **Und-PTT** followed by treatment with 2-isopropoxy-4,4,5,5-tetramethyl-1,3,2-dioxaborolane (IPTMDOB) gave rise to 4,4,5,5-tetramethyl-2-[5′-(4-undec-10-en-1-yl-phenyl)-2,2′-bithien-5-yl]-1,3,2-dioxaborolane (**Und-PTT-Bpin**) in 90% isolated yield. In the next step, a Suzuki cross-coupling reaction between **Und-PTT-BPin** and (4-bromophenyl)(trimethyl)silane led to trimethyl{4-[5′-(4-undec-10-en-1-yl-phenyl)-2,2′-bithien-5-yl]phenyl}silane in 64% isolated yield. The obtained **Und-PTTP-TMS** was used in the hydrosilylation reaction with a 20-fold molar excess of 1,1,3,3-tetramethyldisiloxane (TMDS). Then, the excess of TMDS was removed, and a new portion of **Und-PTTP-TMS** was added to give the desired dimer **D2-Und-PTTP-TMS** in 75% reaction yield. Purification of the dimer was achieved by column chromatography on silica gel followed by recrystallization, leading to chromatographically pure **D2-Und-PTTP-TMS** [as confirmed by thin-layer chromatography (TLC) and gel permeation chromatography (GPC)] in 50% isolated yield. The chemical structures and purities of all precursors and the final compound were confirmed by a combination of ^{1}H, ^{13}C, and ^{29}Si NMR spectroscopy and elemental analysis (see the Experimental Methods section). The compound obtained was highly crystalline as confirmed by differential scanning calorimetry (DSC), which showed reversible melting at the first heating, crystallization at cooling, and crystallization at the second heating, always in the same temperature range: 195−

DOI: 10.1021/acsami.7b01919
ACS Appl. Mater. Interfaces 2017, 9, 18078−18086

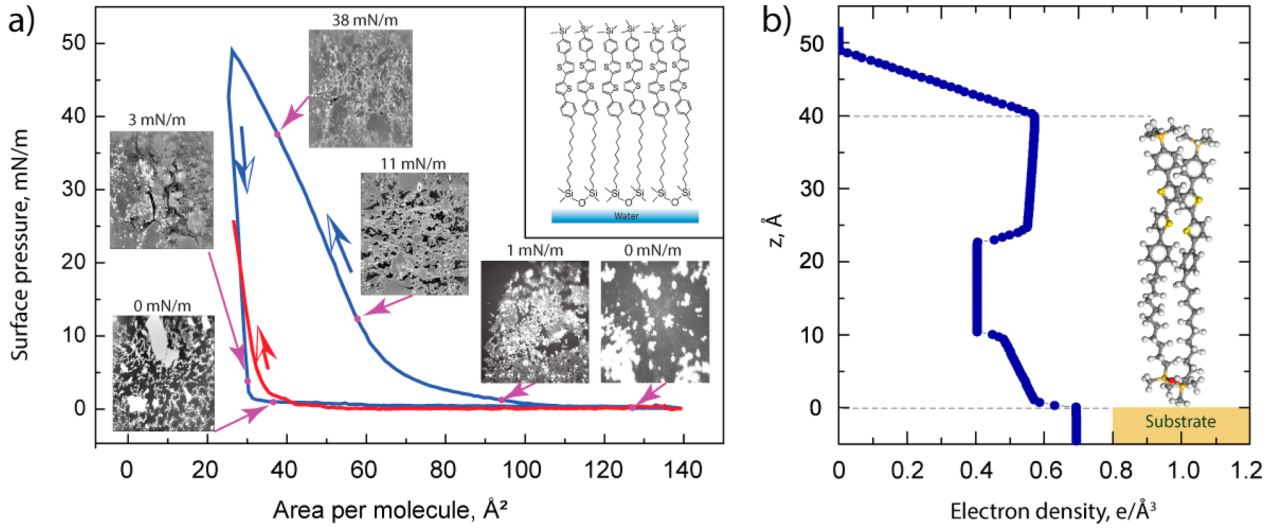

Figure 2. (a) Langmuir isotherm for **D2-Und-PTTP-TMS** (first compression−decompression cycle, blue lines; second compression, red line). BAM micrographs of the Langmuir films are shown at different surface pressures (violet arrows). The inset presents a schematic monolayer packing. (b) Reconstruction of the electron density in the direction perpendicular to the substrate in a Langmuir−Schaefer film and molecular model of **D2-Und-PTTP-TMS** in closed conformation.

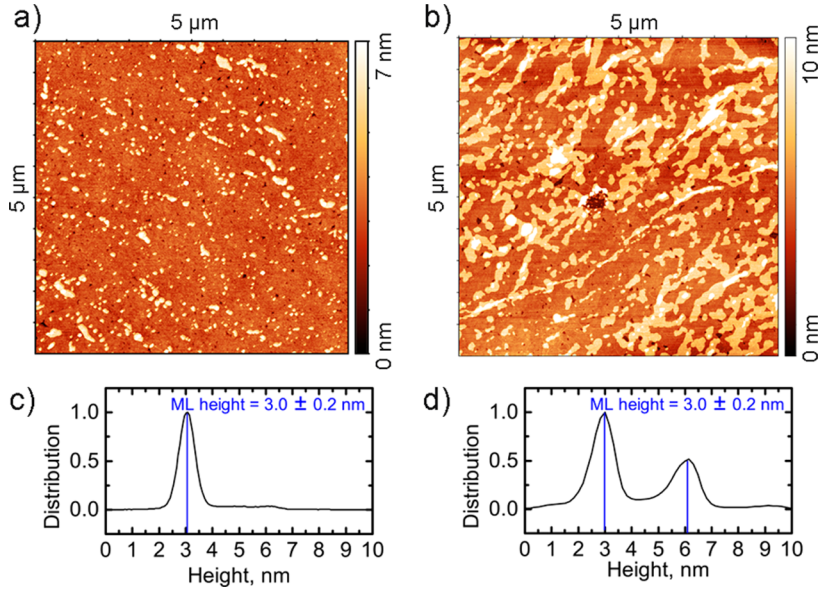

Figure 3. AFM data: topographies of (a) LB and (b) LS films of **D2-Und-PTTP-TMS** on a silicon substrate with the (c,d) corresponding height distributions.

196 °C with an enthalpy of 45−46 J/g [see Figure S8 in the Supporting Information (SI)].

Self-assembly of **D2-Und-PTTP-TMS** on the air−water interface was investigated by the Langmuir technique using Brewster angle microscopy (BAM). The dimer **D2-Und-PTTP-TMS** was stable under normal conditions (in air), did not hydrolyze in the presence of water, and could easily transform from its extended conformation in solution (Figure 1) to the closed conformation on the water surface (Figure 2a shows a scheme of the layer packing) during Langmuir layer formation because of the exceptional flexibility of the disiloxane unit and the possibility of forming hydrogen bonds with water and the high hydrophobicity of the rest of the molecule. Note that the formation of monolayer films based on **D2-Und-PTTP-TMS** by self-assembly from solution directly on the substrate was not possible because this dimer does not have any reactive (e.g., chlorosilyl) anchor groups.

The Langmuir isotherm of the first compression−decompression cycle (blue lines in Figure 2a) was typical for organosilicon derivatives of conjugated oligothiophenes, as was described earlier.[27,29] It has four clearly distinguished regions. The first one, with a surface area of ca. 140−100 Å^2 per molecule, corresponds to the presence of separate islands of molecules not interacting with each other (see Figure 2, Brewster image at 0 mN/m); thus, the surface pressure does not increase with decreasing area. The second region, with a surface area of ca. 100−60 Å^2 per molecule, corresponds to monolayer islands in contact (see Figure 2, Brewster image at 1 mN/m), but the position and tilt angle of the dimer branches ("legs") inside these islands are random, so the surface pressure increases slightly, as the surface area decreases and the dimer

DOI: 10.1021/acsami.7b01919
ACS Appl. Mater. Interfaces 2017, 9, 18078−18086

legs align. The third region, with a surface area of ca. 60−45 Å^2 per molecule, corresponds to the fully covered monolayer with a uniform orientation of PTTP fragments (see Figure 2, Brewster image at 11 mN/m), and it is characterized by a rapid increase of the surface pressure. The fourth region, with a surface area smaller than 45 Å^2 per molecule, corresponds to layer collapse (see Figure 2a, Brewster image at 38 mN/m). It is well-correlated with the theoretically calculated result on the assumption that the dimer molecule has a closed conformation with a nearly vertical orientation of PTTP fragments (molecular model in Figure 2b). We observed a significant hysteresis of the Langmuir isotherm in the compression−decompression cycle, as well as a lack of coincidence in the first and second compressions and no return of the compressed monolayer to the initial state during film decompression. This behavior could be explained by crystallization of the conjugated PTTP units induced by the barrier pressure under layer compression and a delay of repeated spreading under reduced surface pressure. This suggestion can be illustrated by the Brewster micrographs at 3 and 0 mN/m during film decompression (Figure 2a): The images look like "melting crushed ice" with clearly defined edges corresponding to the crushed crystalline monolayer at 3 mN/m that starts to melt at 0 mN/m. It should be noted that the Brewster image at 3 mN/m seems more homogeneous than the Brewster image at 11 mN/m because the crystalline layer under decompression crashes like ice on the river surface: the formed "ice floes" maintain the crystalline structure inside but do not touch each other. That is why we observed a rapid decrease of the surface pressure with persisting layer morphology that differs just by the presence of cracks.

Taking into account our previous X-ray investigations of the similar Langmuir monolayers based on organosilicon oligothiophene derivatives,[27,28] one can expect that the monolayer formed in the region between 60 and 45 Å^2 per molecule is well-ordered (possibly crystalline) and has a vertical uniform orientation of PTTP fragments. This is why Langmuir−Blodgett (LB) and Langmuir−Schaefer (LS) films were transferred at 28 and 30 mN/m (just before layer collapse) to obtain the most perfect monolayer films and at 40 and 42 mN/m (after layer collapse) to obtain films with material excess for postdeposition solvent vapor annealing (see Table S1 in the SI).

The atomic force microscopy (AFM) data (Figure 3) for the LB and LS films confirmed that the morphologies of all of these films were uniform and domainless, with a fully covered bottom monolayer having a thickness of 3.0−3.2 nm (see also Figure S1 in the SI). This value is in good agreement with the theoretically calculated length of the **D2-Und-PTTP-TMS** molecule in its closed conformation (35 Å), which corresponds to a vertical orientation of the PTTP units in the monolayer. Film transfer at surface pressures higher than the collapse pressure (33−35 mN/m) resulted in the appearance of multilayer areas that were not present in the films transferred before monolayer collapse (Figure S1, sample 6, in the SI). Solvent vapor annealing resulted in the disappearance of the multilayers and increased the percentage of monolayer areas (Figure S1, samples 3 and 4 in the SI). By "monolayer areas", we mean the areas with only monolayer coverage compared to the areas with bi- or multilayers. We assign this morphology change to molecular repacking that results in better ordering of the layer.

Grazing-incidence X-ray diffraction (GIXD) studies of the LS films showed an in-plane reflection with a d spacing of 4.76 Å (Figure S2 in the SI). This spacing corresponds to a strong interplanar stacking of PTTP groups absent in the LB film. These data are in accordance with the crystallization induced by Langmuir trough barriers compressing the layer, as was suggested from the Langmuir isotherm. Such induced ordering persists under LS (horizontal) transfer to the substrate but breaks down under LB (vertical) transfer of the monolayer.

X-ray reflectometry (XRR) showed no substantial difference in the structures of the films produced by different techniques (Figure S3 in the SI; the two curves have similar shapes), although the LS film is a slightly thicker (39.8 Å) than the LB film (37.9 Å). The electron density distribution[37] in the direction perpendicular to the substrate (Figure 2b) shows two regions of the films: The closest to the substrate has a density of ∼0.4 Å^{-3}, which is characteristic for aliphatic tails of the molecule, whereas the farthest one is denser (0.55 Å^{-3}) and can be assigned to the aromatic fragments.

To evaluate the semiconducting properties of the LB and LS films, they were transferred onto prestructured Si/SiO_2 substrates with gold electrodes. The LB and LS monolayers deposited on the untreated SiO_2 surface and the spin-cast film did not show any semiconducting properties in OFETs. To reduce the impact of surface traps, dielectric passivation with octyldimethylchlorosilane (ODMS) was applied. Note that LB deposition on ODMS-treated substrates was impossible because of the high surface hydrophobicity of these substrates. Semiconducting properties were found only in the LS monolayers deposited on the ODMS-treated substrate surface. Figure 4 presents the transfer characteristics of the correspond-

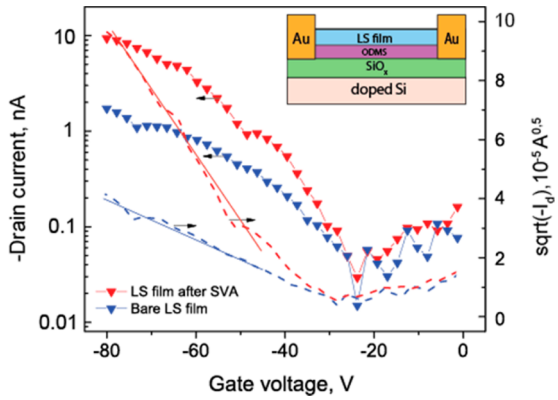

Figure 4. Transfer characteristics of a monolayer LS OFET deposited on an ODMS-treated surface. Straight lines are fits. The saturated mobilities (at V_d = −80 V) were evaluated as 2 × 10^{-6} and 2 × 10^{-5} cm^2/(V s) for the as-prepared and solvent-vapor-annealed samples, respectively.

ing monolayer OFET. The electrical behavior is typical for p-type OFETs, with a hole mobility of 2 × 10^{-6} cm^2/(V s). Postdeposition solvent vapor annealing resulted in a mobility increase to 2 × 10^{-5} cm^2/(V s), which can be assigned to improvements in the morphology of the monolayer. Therefore, the electrical performance of the Langmuir monolayers is well-correlated with their X-ray structure data: Only the well-ordered LS films are semiconducting. Because of this, we present the PL data only for the annealed LS monolayer films. As a reference, we used a polycrystalline spin-cast **D2-Und-PTTP-TMS** sample; its optical microphotograph in circular differential interference contrast (C-DIC) mode is shown in Figure S7a of the SI.

DOI: 10.1021/acsami.7b01919
ACS Appl. Mater. Interfaces 2017, 9, 18078−18086

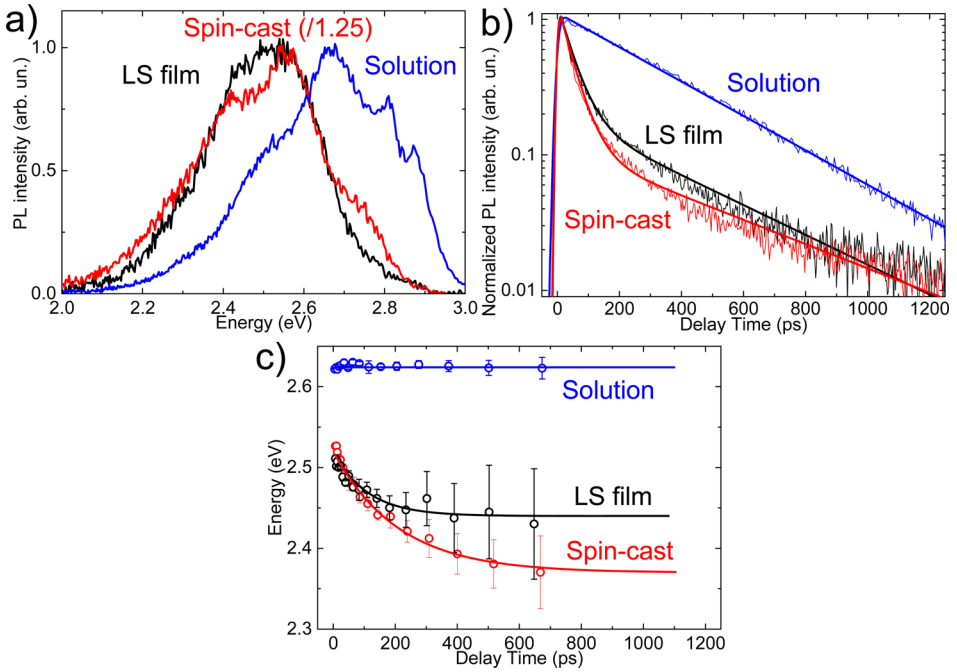

Figure 5. PL data on **D2-Und-PTTP-TMS**. (a) PL spectra, (b) time-resolved kinetics, and (c) spectral diffusions of the LS film (black), 5 g/L toluene solution (blue), and spin-cast sample (red). Scaling between the spectra of the LS film and the spin-cast sample is preserved; the spectrum of **D2-Und-PTTP-TMS** in toluene is arbitrarily normalized. The transients in panel b were obtained by integrating the PL time-resolved maps in the 2.0−3.0 eV spectral range and were normalized to their maxima. The solid lines are mono- or biexponential fits convoluted with the apparatus response of ∼7 ps; the corresponding fit parameters are given in Table S2. In panel c, the time-dependent mean energy of the PL spectrum is shown together with monoexponential fits of $E = E_0 + \Delta E \exp(-t/\tau)$. (For the solution, E_0 = 2.62 eV, and no spectral shift is observed; for the LS film, E_0 = 2.44 eV, ΔE = 80 ± 20 meV, and τ = 110 ± 100 ps; and for the spin-cast film, E_0 = 2.37 eV, ΔE = 150 ± 20 meV, and τ = 210 ± 100 ps.)

To evaluate the PL efficiency in **D2-Und-PTTP-TMS** films, we recorded their PL spectra in an integrating sphere and calculated their PL quantum yields (QYs). The PL QY in the spin-cast sample was ∼1.5%, which is much lower than that in dilute tetrahydrofuran (THF) solution [(21 ± 3)%, Figure S4 in the SI]. Supposedly, the inhomogeneous 3D packing of **D2-Und-PTTP-TMS** in the spin-cast sample results in considerable PL quenching. In contrast, the PL QY in LS films absorbing only (1.6 ± 0.3)% of the light at 405 nm was evaluated as (7 ± 2)%; therefore, the 2D LS film is much more luminescent than the 3D spin-cast film. Thus, we conclude that strong 2D molecular aggregation does not prevent efficient luminescence in the semiconducting monolayers.

To highlight the effects of different packing arrangements of **D2-Und-PTTP-TMS** on its luminescent properties, we compared the PL time-resolved spectra in the annealed LS film, spin-cast sample, and dilute solution (Figure 5). The PL spectrum of the LS film is red-shifted by ∼0.15 eV as compared to that in solution (Figure 5a). The red shift indicates considerable intermolecular interactions in the LS film. The PL of the LS film decayed biexponentially with two characteristic times of ∼50 and ∼420 ps (Figure 5b and Table S2 in the SI). The former is attributed to PL self-quenching due to the densely packed molecules in the film. The longer decay was close to that observed in dilute solution and hence is attributed to the excited-state lifetime (Table S2 in the SI). These results were independent of the substrate treatment with ODMS (Figure S5 in the SI).

The PL spectra of the LS film and the spin-cast sample (Figure 5a) are similar. The latter was slightly broader, which we assign to heterogeneous 3D packing as compared to the ordered 2D packing in the LS film. The PL in the spin-cast sample decays with times similar to those of the LS film; however, the 45-ps component makes a larger contribution. Spectral diffusion in the LS and spin-cast films is much stronger than in solution, which is consistent with the model of thermally activated exciton hopping toward the low-energy sites.[38,39] The magnitude of spectral diffusion in the LS film is noticeably lower than that in the spin-cast sample (Figure 5c; 80 ± 20 meV vs 150 ± 20 meV), in line with improved structural ordering of the LS film. All of these data strongly suggest that reduced PL self-quenching due to structural 2D ordering is the major factor enhancing PL in the LS film.

Interestingly, the PL intensities in the LS film and the spin-cast sample are similar (refer to Figure S6 in the SI for statistics), even though the latter is a factor of ∼50 thicker (the spin-cast sample profile in shown in Figure S7b of the SI). This is consistent with a considerably higher PL QY in the LS film as compared to the spin-cast sample. Therefore, our PL data clearly indicate that the highly ordered 2D molecular packing of **D2-Und-PTTP-TMS** molecules is more beneficial for efficient PL than heterogeneous polycrystalline 3D packing in the spin-cast sample.

CONCLUSIONS

To summarize, we have synthesized and characterized the novel tetramethyldisiloxane dimer **D2-Und-PTTP-TMS**, containing semiconducting oligothiophene−phenylene (**PTTP**) fragments. This material is well-soluble in widely used organic solvents because of its short **PTTP** core and terminal trimethylsilyl groups and is highly stable, allowing for the deposition of Langmuir monolayers at ambient laboratory conditions. We found that 2D packing has a strong effect on the structure and semiconducting properties of the monolayers

DOI: 10.1021/acsami.7b01919
ACS Appl. Mater. Interfaces 2017, 9, 18078−18086

deposited either vertically (LB) or horizontally (LS). The better 2D ordered LS monolayers are semiconducting and exhibit prominent PL, which is significantly more efficient than the PL in the reference polycrystalline 3D spin-cast sample. The PL time-resolved spectra strongly suggest that reduced PL self-quenching due to 2D structural ordering is the major factor enhancing PL in the LS film.

Overall, we have demonstrated that Langmuir monolayers prepared from conjugated organic molecules can combine semiconducting properties and pronounced PL. These findings pave the way to the rational design of functional materials for monolayer organic light-emitting transistors and other optoelectronic devices.

EXPERIMENTAL METHODS

Materials. *n*-Butyl lithium (1.6 M solution in hexane), isopropoxy-4,4,5,5-tetramethyl-1,3,2-dioxaborolane (IPTMDOB), and tetrakis-(triphenylphosphine) palladium(0) [$Pd(PPh_3)_4$] were obtained from Sigma-Aldrich Co. and used without further purification. 1-Bromo-4-undec-10-enyl-benzene was synthesized as described in ref 35. 2-(2,2′-Bithien-5-yl)-4,4,5,5-tetramethyl-1,3,2-dioxaborolane was synthesized according to a literature procedure.[36] (4-Bromophenyl)(trimethyl)-silane was synthesized as described in ref 40. Anhydrous toluene and THF were distilled over CaH_2 under a nitrogen atmosphere before use. All reactions, unless stated otherwise, were carried out under an inert atmosphere using anhydrous solvents. The solvents were removed in a vacuum below 1 Torr at 40 °C.

5-(4-Undec-10-en-1-yl-phenyl)-2,2′-bithiophene (Und-PTT). In an inert atmosphere, degassed solutions of 2-(2,2′-bithien-5-yl)-4,4,5,5-tetramethyl-1,3,2-dioxaborolane (12.95 g, 44 mmol) and 1-bromo-4-undecen-10-yl-benzene (13.00 g, 42 mmol) in a toluene/ethanol mixture (200/20 mL) and a 2 M solution of aqueous Na_2CO_3 (32 mL) were added to $Pd(PPh_3)_4$ (304.00 mg, 0.26 mmol). The reaction mixture was stirred under reflux for 7 h, and then it was cooled to room temperature and poured into 350 mL of water and 500 mL of toluene. The organic phase was separated, washed with water, dried over sodium sulfate, and filtered. The solvent was evaporated in a vacuum, and the residue was dried at 1 Torr. After purification by column chromatography on silica gel (*n*-hexane), **Und-PTT** (13.15 g, 85%) was obtained as a colorless solid. ^{1}H NMR (250 MHz, δ in $CDCl_3$, TMS, ppm): 1.22−1.45 (overlapped peaks with a maximum at 1.28, 12H), 1.67 (m, 2H, J = 7.3 Hz), 2.03 (m, 2H, J = 7.3 Hz), 2.61 (t, 2H, J = 7.3 Hz), 4.95 (m, 2H), 5.80 (m, 1H), 7.03 (dd, 1H, J_1 = 5.0 Hz, J_2 = 3.7 Hz), 7.13 (d, 1H, J = 3.7 Hz), 7.15−7.23 (overlapped peaks with a maximum at 7.17, 5H), 7.51 (dd, 2H, J_1 = 6.5 Hz, J_2 = 1.7 Hz). ^{13}C NMR (75 MHz, δ in $CDCl_3$): 28.92, 29.12, 29.27, 29.47, 29.51, 31.38, 33.80, 35.65, 114.09, 123.16, 123.44, 124.18, 124.53, 125.51, 127.81, 128.94, 131.46, 136.11, 137.55, 139.24, 142.60, 143.36. Calcd (%) for $C_{25}H_{30}S_2$: C, 76.09; H, 7.66; S 16.25. Found: C, 76.21; H, 7.75; S 16.09.

4,4,5,5-Tetramethyl-2-[5′-(4-undec-10-en-1-yl-phenyl)-2,2′-bithien-5-yl]-1,3,2-dioxaborolane (Und-PTT-Bpin). A 2.5 M solution of *n*-butyllithium (3 mL, 7.6 mmol) in hexane was added dropwise to a solution of 5-(4-undec-10-en-1-yl-phenyl)-2,2′-bithiophene (3.00 g, 7,6 mmol) in 100 mL of dry THF at −78 °C. After the reaction mixture had been stirred for 60 min at −78 °C, IPTMDOB (1.55 mL, 7.6 mmol) was added in one portion. The reaction mixture was stirred for 1 h at −78 °C, the cooling bath was removed, and stirring was continued for 1 h. After completion of the reaction, 250 mL of freshly distilled diethyl ether, 150 mL of distilled water, and 7.6 mL of 1 M HCl were added to the reaction mixture. The organic phase was separated, washed with water, dried over sodium sulfate, and filtered. The solvent was evaporated to give 3.85 g (97%) of the 86% product (according GPC analysis) as a white solid. The product was used in the subsequent synthesis without further purification. ^{1}H NMR (250 MHz, δ in $CDCl_3$, TMS, ppm): 1.22−1.32 (overlapped peaks with a maximum at 1.28, 12H), 1.35 (s, 12H), 1.67 (m, 2H, J = 7.3 Hz), 2.03 (m, 2H, J = 7.3 Hz), 2.61 (t, 2H, J = 7.3 Hz), 4.95 (m, 2H Hz), 5.80 (m, 1H), 7.15−7.23 (overlapped peaks with a maximum at 7.17, 5H), 7.50 (d, 2H, J = 8.1 Hz), 7.53 (d, 1H, J = 3.5 Hz). ^{13}C NMR (75 MHz, δ in $CDCl_3$): 24.55, 24.75, 28.91, 29.11, 29.26, 29.47, 29.50, 31.37, 33.80, 35.65, 84.17, 114.09, 123.33, 124.63, 125.23, 125.56, 128.96, 131.38, 135.93, 137.96, 139.23, 142.74, 144.06, 144.25.

Trimethyl{4-[5′-(4-undec-10-en-1-yl-phenyl)-2,2′-bithien-5-yl]phenyl}silane (Und-PTTP-TMS). In an inert atmosphere, degassed solutions of 4,4,5,5-tetramethyl-2-[5′-(4-undec-10-en-1-yl-phenyl)-2,2′-bithien-5-yl]-1,3,2-dioxaborolane (3.0 g, 5.8 mmol) and (4-bromophenyl) (trimethyl)silane (1.17 g, 5.2 mmol) in a toluene/ethanol mixture (80/8 mL) and a 2 M solution of aqueous Na_2CO_3 (10 mL) were added to $Pd(PPh_3)_4$ (333 mg, 0.3 mmol). The reaction mixture was stirred under reflux for 19 h, and then it was cooled to room temperature and poured into 150 mL of water and 250 mL of toluene. The organic phase was separated, washed with water, dried over sodium sulfate, and filtered. The solvent was evaporated in a vacuum, and the residue was dried at 1 Torr. The crude product was purified by being passed through silica gel column (toluene eluent) followed by recrystallization from a toluene/hexane mixture to give pure compound **Und-PTTP-TMS** (1.79 g, 64%) as a yellow solid. ^{1}H NMR (250 MHz, δ in $CDCl_3$, TMS, ppm): 0.28 (s, 9H), 1.22−1.45 (overlapped peaks with a maximum at 1.28, 12H), 1.67 (m, 2H, J = 7.3 Hz), 2.03 (m, 2H, J = 7.3 Hz), 2.61 (t, 2H, J = 7.3 Hz), 4.95 (m, 2H), 5.80 (m, 1H), 7.14 (d, 2H, J = 3.7 Hz), 7.15−7.23 (overlapped peaks with a maximum at 7.17, 3H), 7.24 (d, 1H, J = 0.9 Hz), 7.51 (dd, 2H, J_1 = 6.5 Hz, J_2 = 1.7 Hz), 7.53−7.61 (overlapped peaks with a maximum at 7.57, 4H) . ^{13}C NMR (75 MHz, δ in $CDCl_3$): −1.17, 28.92, 29.12, 29.28, 29.47, 29.52, 31.39, 33.81, 35.66, 114.10, 123.26, 123.86, 124.31, 124.45, 124.78, 125.50, 128.96, 131.44, 133.93, 134.35, 136.12, 136.91, 139.24, 139.90, 142.65, 142.96, 143.40. ^{29}Si NMR (60 MHz, δ in $CDCl_3$): −3.93. Calcd (%) for $C_{34}H_{42}S_2Si$: C, 75.22; H, 7.80; S, 11.81; Si, 5.17. Found: C, 75.91; H, 7.95; S, 11.75, Si, 5.09.

1,3-Bis[11-(4-{5′-[4-(trimethylsilyl)phenyl]-2,2′-bithien-5-yl}-phenyl)undecyl]-1,1,3,3-tetramethyldisiloxane (D2-Und-PTTP-TMS). Trimethyl{4-[5′-(4-undec-10-en-1-ylphenyl)-2,2′-bithien-5-yl]-phenyl}silane (Und-PTTP-TMS) (0.47 g, 0.9 mmol) was dissolved in toluene (20 mL) and 1,1,3,3-tetramethyldisiloxane (3 mL) under argon, after which 25 μL of Karstedt's catalyst was added. The reaction was complete after 3 h of stirring at 60 °C. Then, excess TMDS was removed, and **Und-PTTP-TMS** (0.47 g, 0.9 mmol) was added. The reaction was complete after the solution was stirred at 65 °C for 6 h. The reaction yield according to GPC analysis was 75%. The crude product was purified by being passed through a silica gel column (toluene eluent) followed by recrystallization from toluene/hexane mixture to give pure compound **D2-Und-PTTP-TMS** (0.51 g, 50%) as a yellow solid. ^{1}H NMR (250 MHz, δ in $CDCl_3$, TMS, ppm): 0.03 (s, 12H), 0.29 (s, 18H), 0.54 (t, 4H, J = 7.5 Hz), 1.22−1.45 (overlapped peaks with a maximum at 1.28, 32H), 1.67 (m, 4H, J = 7.3 Hz), 2.61 (t, 4H, J = 7.5 Hz), 7.14 (d, 4H, J = 3.7 Hz), 7.15−7.23 (overlapped peaks with a maximum at 7.17, 6H), 7.24 (d, 2H, J = 0.9 Hz), 7.51 (dd, 4H, J_1 = 6.5 Hz, J_2 = 1.7 Hz), 7.53−7.61 (overlapped peaks with a maximum at 7.57, 8H). ^{13}C NMR (75 MHz, δ in $CDCl_3$): −1.16, 0.40, 18.42, 23.29, 29.34, 29.41, 29.54, 29.62, 29.72, 31.42, 33.45, 35.68, 123.26, 123.86, 124.31, 124.45, 124.78, 125.50, 128.96, 131.43, 133.93, 134.35, 136.12, 136.91, 139.24, 139.89, 142.66, 142.96, 143.40. ^{29}Si NMR (60 MHz, δ in $CDCl_3$): −3.93, 7.33. Anal. Calcd ($C_{72}H_{98}OS_4Si_4$): C, 70.87; H, 8.10; S, 10.51; Si, 9.21. Found: C, 71.01; H, 8.21; S, 10.43; Si, 9.15.

Analytical Techniques. GPC analysis was performed by means of a Shimadzu LC10A^{VP} series chromatograph (Kyoto, Japan) equipped with an RID-10A^{VP} refractometer and SPD-M10A^{VP} diode matrix as detectors and a Phenomenex column (Torrance, CA) with a size of 7.8 × 300 mm^2 filled with Phenogel sorbent with a pour size of 500 Å; THF was used as the eluent. Glassware was dried in a drybox at 150 °C for 2 h, assembled while hot, and cooled in a stream of argon. For thin-layer chromatography, Sorbfil (Russia) plates were used. In the case of column chromatography, silica gel 60 (Merck) was used. ^{1}H NMR spectra were recorded on a Bruker WP-250 SY spectrometer, working at a frequency of 250.13 MHz and utilizing the $CDCl_3$ signal (7.25 ppm) as the internal standard. ^{13}C spectra were recorded using a

DOI: 10.1021/acsami.7b01919
ACS Appl. Mater. Interfaces 2017, 9, 18078−18086

Bruker Avance II 300 spectrometer at 75 MHz. In the case of ^{1}H NMR spectroscopy, the compounds to be analyzed were taken in the form of 1% solutions in $CDCl_3$. The spectra were then processed on the computer using the ACD Laboratories software. Elemental analysis of C, H, and N elements was carried out using a CE 1106 CHN automatic analyzer (Carlo Erba, Cornaredo, Italy). The settling titration using $BaCl_2$ was applied to analyze sulfur. The experimental error was 0.30−0.50%. DSC scans were obtained with a Mettler Toledo DSC30 system at a 20 °C/min heating/cooling rate in the temperature range of 20−300 °C. A nitrogen flow of 50 mL/min was used.

Langmuir, LB, and LS Films. The spreading solution was prepared by dissolving **D2-Und-PTTP-TMS** in toluene at concentrations of 0.33 and 0.5 g/L. The solution was spread on the water surface with a microsyringe, and the film was then left for 5 min to equilibrate before compression started. Data were collected with a Nima 712BAM system using a Teflon trough and barriers at room temperature; the trough area was 900−82 cm^2. Ultrapure water obtained from an Akvilon deionizer D-301 system was used for the subphase with a surface tension of 72.4 mN/m. The monolayers were compressed at a speed equal to 100 mm/min. LB and LS films were obtained by transfer on cleaned silicon substrates with or without gold contacts; some of the substrates were previously treated with octyldimethylchlorosilane (ODMS) from the gas phase for 30 min. The vertical or horizontal dipping method with a dipping speed of 8 mm/min was used to obtain LB or LS monolayer films, respectively. Film transfers were performed at different surface pressures close to the collapse point: (1) at 28 and 30 mN/m (before collapse), corresponding to the most condensed phase in the monolayer, and (2) at 40 and 42 mN/m (after collapse) to have an excess of material on the top of film for solvent vapor annealing.

Substrates. OFETs based on the LB films were prepared on heavily doped silicon substrates with thermally grown oxide as shipped from Ossila Ltd., Sheffield, U.K. The dielectric thickness was 300 nm, and the measured capacitance was 13 nF/cm^2. Before electrode deposition, the factory photoresist was washed off using the manufacturer's recommended procedure. Gold source and drain electrodes were thermally evaporated through a shadow mask. The resulting bottom-gate bottom-contact OFET configuration had a channel width of W = 1000 μm and a length of L = 30 μm. On each substrate, five OFETs were tested.

Spin-Cast Sample. For preparation of the **D2-Und-PTTP-TMS** spin-cast sample, **D2-Und-PTTP-TMS** material was dissolved in toluene at a concentration of 1 g/L. The solution was spin-cast on a glass coverslip substrate at 400 rpm for 120 s.

Thin-Film Characterization. AFM studies were performed with an NT-MDT Solver NEXT instrument in semicontact mode under the ambient environment. Commercially available silicon Bruker FESPA probes with a resonance frequency of 70 kHz were used. The spin-cast film thickness was measured with a surface profilometer (Dektak 6; stylus type with a radius of 12.5 μm and a force of 3 mg). Optical microphotographs were taken using an Axio Imager 2 optical microscope in C-DIC mode (Zeiss).

X-ray Reflectivity and Grazing-Incidence Diffraction. XRR and GIXD studies were performed at the Kurchatov Center for Synchrotron Radiation at the Langmuir station. The energy of the beam was 13.034 keV (λ = 0.947 Å) with $dE/E = 4 \times 10^{-4}$ provided by a 1.7 T bending magnet. A two-crystal Si(111) monochromator yields a flux of 2×10^9 photons s^{-1} (100 mA)$^{-1}$. The size of the beam was 4 × 0.2 mm. A Dectris Mythen detector was used for both reflectivity and grazing-incidence diffraction (GID) scans. The incident angle for GIXD measurements was chosen to be 0.008 Å^{-1}.

The electron density distribution along the normal to the substrate was analyzed using the StochFit program, which utilizes stochastic fitting methods to model the specular reflectivity curves. The calculated distributions of the electron density were later interpolated by multiple-slab models with subsequent solution of the scattering problem and following reconstruction of the reflectivity curves. The electron density was determined as $\rho_e = 2\pi\delta/(\lambda^2\gamma_e)$, where γ_e is the classical electron radius (2.814×10^{-5} Å), δ is the dispersion coefficient, and λ is the X-ray wavelength.

Electrical Measurements. Electrical measurements were performed with a Keithley 2636A source meter in air at room temperature in darkness. Saturated field-effect mobilities were extracted from the transfer characteristics using Shockley's gradual-channel model with a linear fit in the corresponding voltage range. The total measurement time for one curve was about 10 s.

Steady-State Absorption and PL. Absorption and PL spectra of dilute THF solutions (concentrations in the range of 10^{-5}−10^{-6} M) were measured with an ALS01M multifunctional spectrometer.[41] The PL QY was determined using five fluorescence standards with known PL QYs [*p*-terphenyl, phenylphenyloxazole, anthracene, 1,4-bis(5-phenyloxazole-2-yl)phenylene, and rhodamine 6G], whose PL spectra were recorded in optically dilute solutions.[42] The PL QY in solution was calculated as the mean value from the experimental data for each of the five standards. The PL QY in solid samples was measured using the integrating sphere technique reported in ref 43. Briefly, the optical output of a 3.3-in.-diameter integrating sphere (Newport 819C-SL-3.3) was coupled to a spectrometer (InVia, Renishaw). To calibrate the spectral sensitivity of the spectrometer, the sphere was illuminated by an incandescent lamp (SI 8-200 #20; calibrated at the All-Russian Research Institute for Optical and Physical Measurements, Certificate RU 01 no. 643/15). Samples on quartz substrates were excited at 405 nm using a semiconductor laser. The optical response of the substrates was separately verified not to contribute to the PL. The optical absorption of the Langmuir films on quartz substrates at normal incidence was evaluated from their optical transmission in the areas of substrates covered and uncovered by the Langmuir film. For this purpose, a laser beam (405 nm) was transmitted through the samples, and its intensity was recorded with a Si photodetector. The PL spectra of the Langmuir films were recorded under an argon flow in the spectral range of 380−780 nm and averaged over five to seven scans (one scan was recorded for ∼5 min).

Photoluminescence Kinetics. Time-resolved PL kinetics were measured with a streak camera (C5680, Hamamatsu) combined with a polychromator. The samples were excited at a wavelength of 375 nm (3.3 eV) for dilute solutions and 400 nm (3.1 eV) for the LS films and the spin-cast sample by 100 fs pulses produced by the doubled output of a Ti:sapphire laser combined with a 1.9 MHz pulse picker (Coherent Mira). For the dilute solutions, the time-resolved PL was collected in the 90° geometry using a 360-nm long-pass filter (SCHOTT WG360). For the LS films and the spin-cast sample, the time-resolved PL was collected with an inverted microscope (Zeiss Axiovert 100) using a 10×, NA = 0.25 objective, and a 425-nm long-pass dichroic beamsplitter (Chroma T425lpxr); the excitation spot size was ∼5 μm in diameter. In all cases, the apparatus response function was ∼7 ps. To avoid degradation under illumination, the solid samples were purged with nitrogen. All experiments were performed at room temperature.

■ ASSOCIATED CONTENT

Supporting Information

The Supporting Information is available free of charge on the ACS Publications website at DOI: 10.1021/acsami.7b01919.

List of Langmuir films studied and their AFM images, GIXD images, and X-ray reflectometry curves and supplementary PL, optical microscopy, and DSC data (PDF)

■ AUTHOR INFORMATION

Corresponding Authors

*E-mail: ponomarenko@ispm.ru.
*E-mail: paraschuk@gmail.com.

ORCID

Artur A. Mannanov: 0000-0002-3655-2806
Maxim A. Shcherbina: 0000-0002-5569-958X

DOI: 10.1021/acsami.7b01919
ACS Appl. Mater. Interfaces 2017, 9, 18078−18086

Maxim S. Pshenichnikov: 0000-0002-5446-4287
Sergei A. Ponomarenko: 0000-0003-0930-7722

Author Contributions

E.V.A. prepared and characterized Langmuir films, A.A.M. and O.V.K. performed time-resolved PL experiments, A.S.S. made AFM and electrical characterizations of the monolayer films, O.V. and O.V.B. synthesized the materials, A.V.B. and M.A.S. made XRD experiments, S.N.C. analyzed the XRD data, V.G.K. and V.V.D. measured the PL QY, O.V.K. prepared and analyzed spin-cast samples, M.S.P. planned and supervised the time-resolved PL experiments, D.Y.P. and S.A.P. supervised the project. The manuscript was written through contributions of all the authors. All authors have given approval to the final version of the manuscript.

Notes

The authors declare no competing financial interest.

■ ACKNOWLEDGMENTS

This work was supported by the Russian Science Foundation (Grant 15-02-30031). We thank S. Yakunin and A. Rogachev at the Langmuir station (Kurchatov Institute, Moscow, Russia) for their assistance during the synchrotron measurements, O. Parashchuk for her help in processing the PL QY data, G. V. Cherkaev for NMR measurements, and P. V. Dmitryakov for DSC measurements. PL QY measurements were performed on equipment purchased under the Lomonosov Moscow State University Program of Development.

■ REFERENCES

(1) Andringa, A. M.; Spijkman, M. J.; Smits, E. C. P.; Mathijssen, S. G. J.; van Hal, P. A.; Setayesh, S.; Willard, N. P.; Borshchev, O. V.; Ponomarenko, S. A.; Blom, P. W. M.; de Leeuw, D. M. Gas Sensing with Self-Assembled Monolayer Field-Effect Transistors. *Org. Electron.* **2010**, *11*, 895−898.

(2) Mulla, M. Y.; Tuccori, E.; Magliulo, M.; Lattanzi, G.; Palazzo, G.; Persaud, K.; Torsi, L. Capacitance-Modulated Transistor Detects Odorant Binding Protein Chiral Interactions. *Nat. Commun.* **2015**, *6*, 6010.

(3) Dumitru, L. M.; Manoli, K.; Magliulo, M.; Palazzo, G.; Torsi, L. Low-Voltage Solid Electrolyte-Gated OFETs for Gas Sensing Applications. *Microelectron. J.* **2014**, *45*, 1679−1683.

(4) Casalini, S.; Leonardi, F.; Cramer, T.; Biscarini, F. Organic Field-Effect Transistor for Label-Free Dopamine Sensing. *Org. Electron.* **2013**, *14*, 156−163.

(5) Casalini, S.; Dumitru, A. C.; Leonardi, F.; Bortolotti, C. A.; Herruzo, E. T.; Campana, A.; de Oliveira, R. F.; Cramer, T.; Garcia, R.; Biscarini, F. Multiscale Sensing of Antibody-Antigen Interactions by Organic Transistors and Single-Molecule Force Spectroscopy. *ACS Nano* **2015**, *9*, 5051−5062.

(6) Klauk, H.; Zschieschang, U.; Pflaum, J.; Halik, M. Ultralow-Power Organic Complementary Circuits. *Nature* **2007**, *445*, 745−748.

(7) Baeg, K. J.; Jung, S. W.; Khim, D.; Kim, J.; Kim, D. Y.; Koo, J. B.; Quinn, J. R.; Facchetti, A.; You, I. K.; Noh, Y. Y. Low-Voltage, High Speed Inkjet-Printed Flexible Complementary Polymer Electronic Circuits. *Org. Electron.* **2013**, *14*, 1407−1418.

(8) Mandal, S.; Dell'Erba, G.; Luzio, A.; Bucella, S. G.; Perinot, A.; Calloni, A.; Berti, G.; Bussetti, G.; Duò, L.; Facchetti, A.; Noh, Y.-Y.; Caironi, M. Fully-Printed, All-Polymer, Bendable and Highly Transparent Complementary Logic Circuits. *Org. Electron.* **2015**, *20*, 132−141.

(9) Yu, H.; Bao, Z.; Oh, J. H. High-Performance Phototransistors Based on Single-Crystalline n-Channel Organic Nanowires and Photogenerated Charge-Carrier Behaviors. *Adv. Funct. Mater.* **2013**, *23*, 629−639.

(10) Smithson, C. S.; Wu, Y.; Wigglesworth, T.; Zhu, S. A More Than Six Orders of Magnitude UV-Responsive Organic Field-Effect Transistor Utilizing a Benzothiophene Semiconductor and Disperse Red 1 For Enhanced Charge Separation. *Adv. Mater.* **2015**, *27*, 228−233.

(11) Smithson, C. S.; Ljubic, D.; Wu, Y.; Zhu, S. Rapid UV-A Photo Detection Using a BTBT Organic Thin-Film Transistor Enhanced by a 1,5-Dichloro-9,10-Dintiro-Anthracene Acceptor. *Org. Electron.* **2016**, *37*, 42−46.

(12) Capelli, R.; Toffanin, S.; Generali, G.; Usta, H.; Facchetti, A.; Muccini, M. Organic Light-Emitting Transistors with an Efficiency That Outperforms the Equivalent Light-Emitting Diodes. *Nat. Mater.* **2010**, *9*, 496−503.

(13) Muccini, M.; Koopman, W.; Toffanin, S. The Photonic Perspective of Organic Light-Emitting Transistors. *Laser Photonics Rev.* **2012**, *6*, 258−275.

(14) Zhang, C.; Chen, P.; Hu, W. Organic Light-Emitting Transistors: Materials, Device Configurations, and Operations. *Small* **2016**, *12*, 1252−1294.

(15) Borshchev, O. V.; Ponomarenko, S. A. Self-Assembled Organic Semiconductors for Monolayer Field-Effect Transistors. *Polym. Sci., Ser. C* **2014**, *56*, 32−46.

(16) Mottaghi, M.; Lang, P.; Rodriguez, F.; Rumyantseva, A.; Yassar, A.; Horowitz, G.; Lenfant, S.; Tondelier, D.; Vuillaume, D. Low-Operating-Voltage Organic Transistors Made of Bifunctional Self-Assembled Monolayers. *Adv. Funct. Mater.* **2007**, *17*, 597−604.

(17) Smits, E. C. P.; Mathijssen, S. G. J.; van Hal, P. A.; Setayesh, S.; Geuns, T. C. T.; Mutsaers, K. A. H. A.; Cantatore, E.; Wondergem, H. J.; Werzer, O.; Resel, R.; Kemerink, M.; Kirchmeyer, S.; Muzafarov, A. M.; Ponomarenko, S. A.; de Boer, B.; Blom, P. W. M.; de Leeuw, D. M. Bottom-Up Organic Integrated Circuits. *Nature* **2008**, *455*, 956−959.

(18) Mathijssen, S. G. J.; Smits, E. C. P.; van Hal, P. A.; Wondergem, H. J.; Ponomarenko, S. A.; Moser, A.; Resel, R.; Bobbert, P. A.; Kemerink, M.; Janssen, R. A. J.; de Leeuw, D. M. Monolayer Coverage and Channel Length Set the Mobility in Self-Assembled Monolayer Field-Effect Transistors. *Nat. Nanotechnol.* **2009**, *4*, 674−680.

(19) Ponomarenko, S. A.; Borshchev, O. V.; Meyer-Friedrichsen, T.; Pleshkova, A. P.; Setayesh, S.; Smits, E. C. P.; Mathijssen, S. G. J.; de Leeuw, D. M.; Kirchmeyer, S.; Muzafarov, A. M. Synthesis of Monochlorosilyl Derivatives of Dialkyloligothiophenes for Self-Assembling Monolayer Field-Effect Transistors. *Organometallics* **2010**, *29*, 4213−4226.

(20) Lenz, T.; Schmaltz, T.; Novak, M.; Halik, M. Self-Assembled Monolayer Exchange Reactions as a Tool for Channel Interface Engineering in Low-Voltage Organic Thin-Film Transistors. *Langmuir* **2012**, *28*, 13900−13904.

(21) Schmaltz, T.; Amin, A. Y.; Khassanov, A.; Meyer-Friedrichsen, T.; Steinruck, H. G.; Magerl, A.; Segura, J. J.; Voitchovsky, K.; Stellacci, F.; Halik, M. Low-Voltage Self-Assembled Monolayer Field-Effect Transistors on Flexible Substrates. *Adv. Mater.* **2013**, *25*, 4511−4514.

(22) Gholamrezaie, F.; Kirkus, M.; Mathijssen, S. G. J.; de Leeuw, D. M.; Meskers, S. C. J. Photophysics of Self-Assembled Monolayers of a pi-Conjugated Quinquethiophene Derivative. *J. Phys. Chem. A* **2012**, *116*, 7645−7650.

(23) Yamao, T.; Shimizu, Y.; Terasaki, K.; Hotta, S. Organic Light-Emitting Field-Effect Transistors Operated by Alternating-Current Gate Voltages. *Adv. Mater.* **2008**, *20*, 4109−4112.

(24) Bisri, S. Z.; Takenobu, T.; Yomogida, Y.; Shimotani, H.; Yamao, T.; Hotta, S.; Iwasa, Y. High Mobility and Luminescent Efficiency in Organic Single-Crystal Light-Emitting Transistors. *Adv. Funct. Mater.* **2009**, *19*, 1728−1735.

(25) Hotta, S.; Yamao, T. The Thiophene/Phenylene Co-Oligomers: Exotic Molecular Semiconductors Integrating High-Performance Electronic and Optical Functionalities. *J. Mater. Chem.* **2011**, *21*, 1295−1304.

(26) Agina, E. V.; Usov, I. A.; Borshchev, O. V.; Wang, J.; Mourran, A.; Shcherbina, M. A.; Bakirov, A. V.; Grigorian, S.; Möller, M.; Chvalun, S. N.; Ponomarenko, S. A. Formation of Self-Assembled

DOI: 10.1021/acsami.7b01919
ACS Appl. Mater. Interfaces 2017, 9, 18078−18086

Organosilicon-Functionalized Quinquethiophene Monolayers by Fast Processing Techniques. *Langmuir* **2012**, *28*, 16186−16195.
(27) Sizov, A. S.; Anisimov, D. S.; Agina, E. V.; Borshchev, O. V.; Bakirov, A. V.; Shcherbina, M. A.; Grigorian, S.; Bruevich, V. V.; Chvalun, S. N.; Paraschuk, D. Y.; Ponomarenko, S. A. Easily Processable Highly Ordered Langmuir-Blodgett Films of Quaterthiophene Disiloxane Dimer for Monolayer Organic Field-Effect Transistors. *Langmuir* **2014**, *30*, 15327−15334.
(28) Sizov, A. S.; Agina, E. V.; Gholamrezaie, F.; Bruevich, V. V.; Borshchev, O. V.; Paraschuk, D. Y.; de Leeuw, D. M.; Ponomarenko, S. A. Oligothiophene-Based Monolayer Field-Effect Transistors Prepared by Langmuir-Blodgett Technique. *Appl. Phys. Lett.* **2013**, *103*, 043310.
(29) Agina, E. V.; Sizov, A. S.; Anisimov, D. S.; Trul, A. A.; Borshchev, O. V.; Paraschuk, D. Y.; Shcherbina, M. A.; Chvalun, S. N.; Ponomarenko, S. A. Thiophene-Based Monolayer Ofets Prepared by Langmuir Techniques. *Proc. SPIE* **2015**, *9568*, 95680Z.
(30) Borshchev, O. V.; Sizov, A. S.; Agina, E. V.; Bessonov, A. A.; Ponomarenko, S. A. Synthesis of Organosilicon Derivatives of [1]Benzothieno[3,2-B][1]-Benzothiophene Enabling Efficient Monolayer Langmuir-Blodgett Organic Field Effect Transistors. *Chem. Commun.* **2017**, *53*, 885−888.
(31) Yam, V. W.-W.; Au, V. K.-M.; Leung, S. Y.-L. Light-Emitting Self-Assembled Materials Based on d^8 and d^{10} Transition Metal Complexes. *Chem. Rev.* **2015**, *115*, 7589−7728.
(32) Pal, A. J.; Paloheimo, J.; Stubb, H. Molecular Light-Emitting Diodes Using Quinquethiophene Langmuir-Blodgett Films. *Appl. Phys. Lett.* **1995**, *67*, 3909−3911.
(33) Pal, A. J.; Östergård, T.; Paloheimo, J.; Stubb, H. Polymeric Light-Emitting Diodes from Molecularly Thin Poly(3-Hexylthiophene) Langmuir-Blodgett Films. *Appl. Phys. Lett.* **1996**, *69*, 1137−1139.
(34) Pal, A. J.; Österbacka, T.; Källman, K.-M.; Stubb, H. Transient Electroluminescence: Mobility and Response Time in Quinquethiophene Langmuir-Blodgett Films. *Appl. Phys. Lett.* **1997**, *71*, 228−230.
(35) Janssen, P. G. A.; Pouderoijen, M.; van Breemen, A. J. J. M.; Herwig, P. T.; Koeckelberghs, G.; Popa-Merticaru, A. R.; Meskers, S. C. J.; Valeton, J. J. P.; Meijer, E. W.; Schenning, A. P. H. J. Synthesis and Properties of α,ω-Phenyl-Capped Bithiophene Derivatives. *J. Mater. Chem.* **2006**, *16*, 4335−4342.
(36) Huang, C. H.; McClenaghan, N. D.; Kuhn, A.; Hofstraat, J. W.; Bassani, D. M. Enhanced Photovoltaic Response in Hydrogen-Bonded All-Organic Devices. *Org. Lett.* **2005**, *7*, 3409−3412.
(37) Shcherbina, M. A.; Chvalun, S. N.; Ponomarenko, S. A.; Kovalchuk, M. V. Modern Approaches to Investigation of Thin Films and Monolayers: X-Ray Reflectivity, Grazing-Incidence X-Ray Scattering and X-Ray Standing Waves. *Russ. Chem. Rev.* **2014**, *83*, 1091−1119.
(38) Mikhnenko, O. V.; Blom, P. W. M.; Nguyen, T.-Q. Exciton Diffusion in Organic Semiconductors. *Energy Environ. Sci.* **2015**, *8*, 1867−1888.
(39) Köhler, A.; Bassler, H. *Electronic Processes in Organic Semiconductors: An Introduction*; Wiley-VCH: Weinheim, Germany, 2015.
(40) Postnikov, V. A.; Odarchenko, Y. I.; Iovlev, A. V.; Bruevich, V. V.; Pereverzev, A. Y.; Kudryashova, L. G.; Sobornov, V. V.; Vidal, L.; Chernyshov, D.; Luponosov, Y. N.; Borshchev, O. V.; Surin, N. M.; Ponomarenko, S. A.; Ivanov, D. A.; Paraschuk, D. Yu. Molecularly Smooth Single-Crystalline Films of Thiophene−Phenylene Co-Oligomers Grown at the Gas−Liquid Interface. *Cryst. Growth Des.* **2014**, *14*, 1726−1737.
(41) Shumilkina, E. A.; Borshchev, O. V.; Ponomarenko, S. A.; Surin, N. M.; Pleshkova, A. P.; Muzafarov, A. M. Synthesis and Optical Properties of Linear and Branched Bithienylsilanes. *Mendeleev Commun.* **2007**, *17*, 34−36.
(42) Brouwer, A. M. Standards for Photoluminescence Quantum Yield Measurements in Solution (IUPAC Technical Report). *Pure Appl. Chem.* **2011**, *83*, 2213−2228.
(43) Kazantsev, M. S.; Frantseva, E. S.; Kudriashova, L. G.; Konstantinov, V. G.; Mannanov, A. A.; Rybalova, T. V.; Karpova, E. V.; Shundrina, I. K.; Kamaev, G. N.; Pshenichnikov, M. S.; Mostovich, E. A.; Paraschuk, D. Yu. Highly-Emissive Solution-Grown Furan/Phenylene Co-Oligomer Single Crystals. *RSC Adv.* **2016**, *6*, 92325−92329.

DOI: 10.1021/acsami.7b01919
ACS Appl. Mater. Interfaces 2017, 9, 18078−18086